




Article

The crystal structures of the mixed-valence tellurium oxysalts tlalallite, $(\text{Ca,Pb})_3\text{CaCu}_6[\text{Te}_3^{4+}\text{Te}^{6+}\text{O}_{12}]_2(\text{Te}^{4+}\text{O}_3)_2(\text{SO}_4)_2 \cdot 3\text{H}_2\text{O}$, and carlfriesite, $\text{CaTe}_2^{4+}\text{Te}^{6+}\text{O}_8$

Owen P. Missen^{1,2*} , Anthony R. Kampf³, Stuart J. Mills¹, Robert M. Housley⁴, John Spratt⁵, Mark D. Welch⁶, Mark F. Coolbaugh⁷, Joe Marty⁸, Marek Chorazewicz⁹ and Cristiano Ferraris¹⁰

¹Geosciences, Museums Victoria, GPO Box 666, Melbourne 3001, Victoria, Australia; ²School of Earth, Atmosphere and Environment, 9 Rainforest Walk, Monash University, Clayton 3800, Victoria, Australia; ³Mineral Sciences Department, Natural History Museum of Los Angeles County, 900 Exposition Boulevard, Los Angeles, CA 90007, USA; ⁴Division of Geological and Planetary Sciences, California Institute of Technology, Pasadena, CA 91125, USA; ⁵Department of Core Research Laboratories, Natural History Museum, Cromwell Road, London SW7 5BD, UK; ⁶Department of Earth Sciences, Natural History Museum, Cromwell Road, London SW7 5BD, UK; ⁷Renaissance Gold Inc., 4750 Longley Lane, Suite 106, Reno, NV 89502, USA; ⁸5199 East Silver Oak Road, Salt Lake City, UT 84108, USA; ⁹124 Pineplank Lane, Simi Valley, CA 93065, USA; and ¹⁰Laboratoire de Physique des Milieux Condensés (LPMC), CNRS-UMR 7590, Muséum National d'Histoire Naturelle (MNHN), 61 rue Buffon, 75005 Paris, France

ABSTRACT

The crystal structure of tlalallite has been determined using single-crystal X-ray diffraction and supported by electron probe micro-analysis, powder diffraction and Raman spectroscopy. Tlalallite is trigonal, space group $P321$, with $a = 9.1219(17)$ Å, $c = 11.9320(9)$ Å and $V = 859.8(3)$ Å³, and was refined to $R_1 = 0.0296$ for 786 reflections with $I > 2\sigma(I)$. This study resulted from the discovery of well-crystallised tlalallite at the Wildcat prospect, Utah, USA. The chemical formula of tlalallite has been revised to $(\text{Ca,Pb})_3\text{CaCu}_6[\text{Te}_3^{4+}\text{Te}^{6+}\text{O}_{12}]_2(\text{Te}^{4+}\text{O}_3)_2(\text{SO}_4)_2 \cdot 3\text{H}_2\text{O}$, or more simply $(\text{Ca,Pb})_3\text{CaCu}_6\text{Te}_8^{4+}\text{Te}_2^{6+}\text{O}_{30}(\text{SO}_4)_2 \cdot 3\text{H}_2\text{O}$, from $\text{H}_6(\text{Ca,Pb})_2(\text{Cu,Zn})_3(\text{TeO}_3)_4(\text{TeO}_6)(\text{SO}_4)$. The tlalallite structure consists of layers containing distorted Cu^{2+}O_6 octahedra, Te^{6+}O_6 octahedra and Te^{4+}O_4 disphenoids (which together form the new mixed-valence phyllostellurate anion $[\text{Te}_3^{4+}\text{Te}^{6+}\text{O}_{12}]^{12-}$), Te^{4+}O_3 trigonal pyramids and CaO_8 polyhedra. SO_4 tetrahedra, $\text{Ca}(\text{H}_2\text{O})_3\text{O}_6$ polyhedra and H_2O groups fill the space between the layers. Tlalallite is only the second naturally occurring compound containing tellurium in both the 4^+ and 6^+ oxidation states with a known crystal structure, the other being carlfriesite, $\text{CaTe}_2^{4+}\text{Te}^{6+}\text{O}_8$. Carlfriesite is the predominant secondary tellurium mineral at the Wildcat prospect. We also present an updated structure for carlfriesite, which has been refined to $R_1 = 0.0230$ for 874 reflections with $I > 2\sigma(I)$. This updated structural refinement improves upon the one reported previously by refining all atoms anisotropically and presenting models of bond valence and Te^{4+} secondary bonding.

Keywords: tlalallite, crystal structure, tellurate, tellurite, mixed-valence tellurium, carlfriesite, oxysalt, Wildcat prospect, Moctezuma

(Received 13 December 2018; accepted 21 January 2019; Accepted Manuscript online: 12 February 2019; Associate Editor: Oleg I Siidra)

Introduction

Although typically rare, tellurium (Te) oxysalt minerals often have unique structures, many of which have neither been determined nor synthesised (Christy *et al.*, 2016a). The rate of discovery of Te oxysalts has burgeoned in the last decade, aided greatly by the discovery of new Te mineral localities, including at Otto Mountain and the Blue Bell mine in the Mojave desert, near Baker, California (Marty *et al.*, 2010; Mills *et al.*, 2014; Christy *et al.*, 2016b) and the Masonic Mountain district mines in northern California (Kampf *et al.*, 2018). Tellurium oxysalt compounds are continuing to grow as an area of interest, in part due to the rich structural variation of Te bonding (e.g. Mills

and Christy, 2013). Tellurites (Te^{4+} oxysalts), especially synthetic analogues, have been investigated more thoroughly due to the asymmetrically bonded Te^{4+} cation (Christy and Mills, 2013; Brugger *et al.*, 2016); the inclusion of which allows for greater structural versatility than the more regularly coordinated Te^{6+} , including the possibility of generating non-linear optical properties (Weil *et al.*, 2018).

Mixed-valence Te oxysalts are uncommon as they require very specific conditions in which the tellurite and tellurate anions are stable enough to crystallise together. At surface conditions (25°C, ambient pressure), the border of stability between Te^{4+} and Te^{6+} occurs for $\log f_{\text{O}_2}$ values between -10 and 0 across a pH range of 0 to 14 (McPhail, 1995; Grundler *et al.*, 2013). Tlalallite is a rare secondary Te mineral found at only a few North American localities and is one of many Te oxysalt minerals first recognised from the Moctezuma, Bambolla, Bambollita and Oriental mines of Sonora, Mexico (Williams and Duggan, 1978). Pb-rich tlalallite was discovered concurrently at Tombstone, Arizona. Since then, tlalallite has also been identified at other mines, including Otto

*Author for correspondence: Owen P. Missen, Email: omissen@museum.vic.gov.au

Cite this article: Missen O.P., Kampf A.R., Mills S.J., Housley R.M., Spratt J., Welch M.D., Coolbaugh M.F., Marty J., Chorazewicz M. and Ferraris C. (2019) The crystal structures of the mixed-valence tellurium oxysalts tlalallite, $(\text{Ca,Pb})_3\text{CaCu}_6[\text{Te}_3^{4+}\text{Te}^{6+}\text{O}_{12}]_2(\text{Te}^{4+}\text{O}_3)_2(\text{SO}_4)_2 \cdot 3\text{H}_2\text{O}$, and carlfriesite, $\text{CaTe}_2^{4+}\text{Te}^{6+}\text{O}_8$. *Mineralogical Magazine* 83, 539–549. <https://doi.org/10.1180/mgm.2019.9>



Fig. 1. Pale emerald-green crystalline aggregates of tlapallite from Wildcat Prospect on specimen number 67231, closely associated with carlfriesite (yellow) and quartz. Field of view = 0.84 mm.



Fig. 2. Pale yellow transparent crystals of carlfriesite from Wildcat Prospect on specimen number 67227. Field of view = 3.5 mm.



Fig. 3. Back-scattered electron image of one of the grains used in the Caltech microprobe analyses of tlapallite from Wildcat Prospect. Field of view is 100 μ m. EDS analyses were recorded at the numbered spots. Spots 16, 17, 18, and 22 are tlapallite blades. Spot 19 is carlfriesite. Spots 20, 21, and 23 are fine-grained mixtures of the two.

Table 1. The average composition of tlapallite determined by electron probe micro-analysis and structure determination.

Oxide	Cotype, Moctezuma (specimen number 180.92) 15 analyses				Wildcat prospect, Utah (specimen number 67231) 14 analyses			
	Avg.	Min.	Max.	S.D.	Avg.	Min.	Max.	S.D.
SiO ₂	0.08	0	0.24	0.10			N.A.	
SO ₃	4.53	4.19	4.82	0.17	6.14	5.99	6.37	0.11
CaO	7.86	7.49	8.36	0.24	7.99	7.60	8.53	0.31
CuO	15.8	14.9	16.5	0.17	17.46	17.14	17.72	0.16
ZnO	1.57	0.84	2.03	0.29			N.D.	
As ₂ O ₅	0.54	0.29	0.86	0.14			N.D.	
Sb ₂ O ₅			N.A.		1.48	0.87	1.90	0.37
TeO ₂ *	47.5	46.4	48.7	0.62	47.34	45.90	48.04	0.55
TeO ₃ *	13.0	12.7	13.4	0.17	10.38	9.77	11.16	0.43
PbO	4.32	3.14	6.02	0.91	0.96	0.73	1.21	0.16
H ₂ O**	1.97	1.93	2.01	0.03	2.03	1.97	2.07	0.02
Total	97.18				93.77			

* Te total split in a 4:1 ratio of TeO₂:TeO₃ for cotype tlapallite, calculated from the crystal structure, while the 4:1 split for Wildcat prospect takes Sb₂O₅ into account
** Calculated based on the crystal structure (using 41 total O atoms per formula unit as a reference)
N.A. – Not analysed; N.D. – Not determined; S.D. – standard deviation.

Mountain, California and the North Star mine, Utah, and is thus more widespread than many other Te oxysalts. Tlapallite commonly occurs in association with carlfriesite (Williams and Gaines, 1975) – the only other naturally occurring mixed-valence Te oxysalt with a known crystal structure (Effenberger *et al.*, 1978). Tlapallite, occurring as powdery, paint-like coatings, was first described without a crystal structure (Williams and Duggan, 1978). The end-member formula was reported as H₆Ca₂Cu₃(TeO₃)₄(TeO₆)(SO₄), or more generally H₆(Ca,Pb)₂(Cu,Zn)₃(TeO₃)₄(TeO₆)(SO₄). The Te oxidation states and ratio of Te⁴⁺:Te⁶⁺ were determined by wet chemical methods (Williams and Duggan, 1978).

Carlfriesite was first identified from the Bambollita mine, Moctezuma (Williams and Gaines, 1975). First defined as containing only Te⁴⁺, the mineral was successfully synthesised and discovered to contain Te in both oxidation states (Effenberger *et al.*, 1978). It was amongst the first handful of compounds to have this feature, following the synthesis of Te⁴⁺Te⁶⁺O₅ five years earlier (Lindqvist and Moret, 1973). Recently, ‘girdite’, which has since been discredited (Kampf *et al.*, 2017) and eztlite, which was recently redefined by Missen *et al.* (2018), have been found not to be mixed-valence Te oxysalts, leaving (aside from tlapallite and carlfriesite) only three other minerals of this type. None of these three has a known crystal structure: oboyerite (Williams, 1979), tlalocite (Williams, 1975) and yecoraite (Williams and Cesbron, 1985). Oboyerite typically forms ball-like growths, which seem to be composed of a mixture of phases based on a preliminary study incorporating some of the authors (OPM, ARK and SJM). Tlalocite and yecoraite are only known as powdery coatings, meaning that it will be difficult to determine the structures until more crystalline occurrences are found. Until these minerals have been investigated in greater detail, their status as mixed-valence Te oxysalts must be considered doubtful.

The present study is part of a broader one aimed at determining crystal structures for the ~20 secondary Te minerals without a known topology, based on Christy *et al.* (2016a) and the official International Mineralogical Association (IMA) list of minerals (Pasero, 2018). There is a high likelihood that many of them

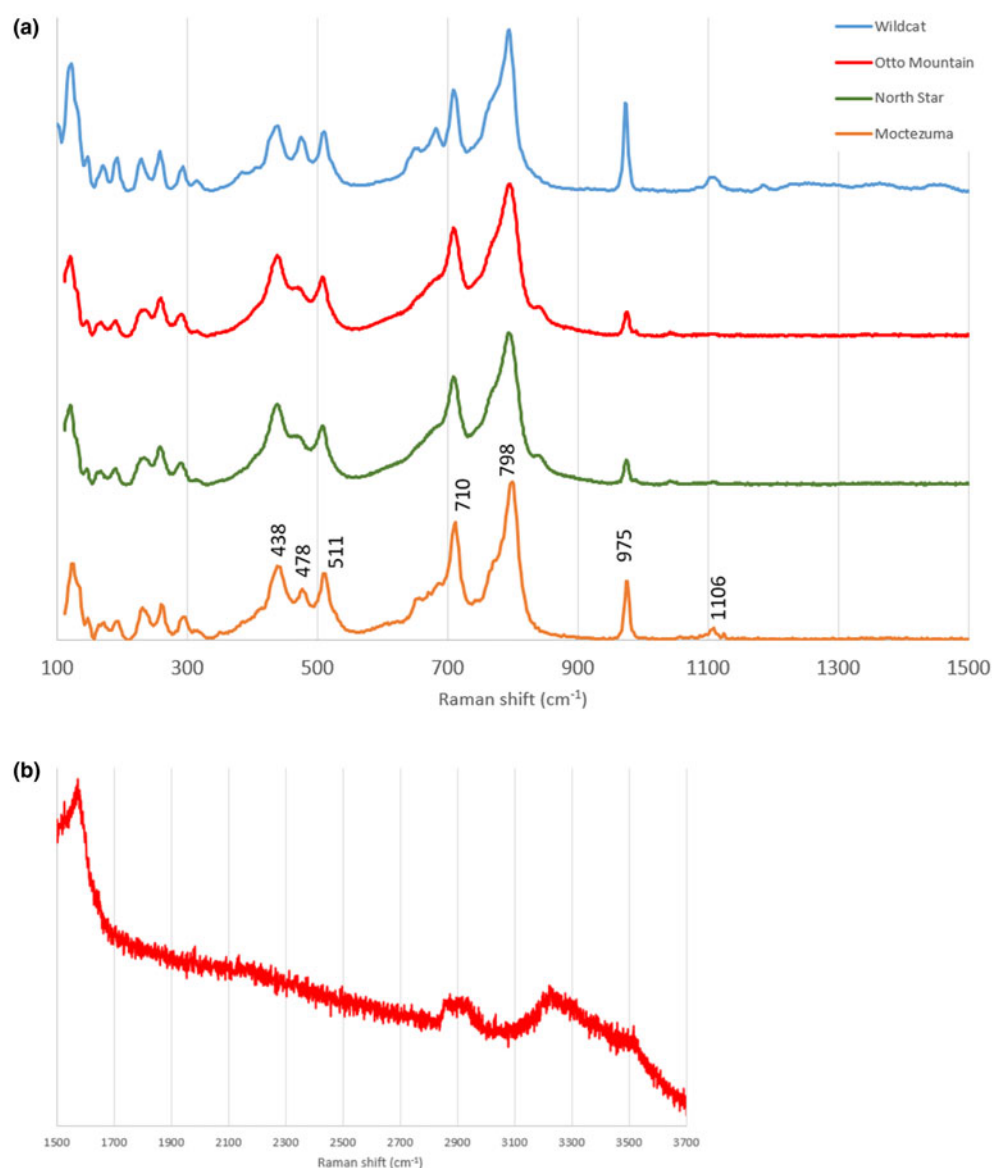


Fig. 4. (a) Raman spectra of tlapallite from the four analysed localities, with key lines identified for the Moctezuma specimen. All units in cm^{-1} . (b) Raman spectrum of Otto Mountain tlapallite between 1500 and 3700 cm^{-1} .

will possess a unique structural arrangement, consistent with the majority of known secondary Te mineral structures having no known synthetic analogue at their time of discovery. For instance, the high charge of Te^{6+} coupled with the other cations it is likely to be associated with (e.g. Cu^{2+} and Pb^{2+}) results in a diverse range of tellurates. The factors governing the variety of Te oxysalts found today are fully discussed in Christy *et al.* (2016a).

Specimen and locality descriptions

Grains of cotype tlapallite from the Muséum Nationale d'Histoire Naturelle (MNHN), Paris collection (MNHN_MIN_180.92, henceforth referred to as 180.92) were first examined. This material originates from Bambollita Mine (Oriental Mine), Moctezuma, Sonora, Mexico; the sample was part of a suite of 35 samples originally described by Sidney Williams and bought by the MNHN after the IMA congress in Orléans (France) in 1980. Due to the powdery nature of cotype tlapallite, the crystal structure could not be

determined. Powder X-ray diffraction (PXRD), Raman analysis and electron probe microanalysis (EPMA) were used to verify its identity. A high-quality Raman spectrum was recorded and was subsequently entered into the Caltech Raman database (see details below). This was then used for comparison with material from several Te-rich localities.

In the course of this study, tlapallite specimens have been identified from four localities (Bambollita mine, Moctezuma, Sonora, Mexico; Otto Mountain, California, USA; North Star mine, Utah, USA; and Wildcat prospect, Utah, USA), confirming the distinctive identity of what until now has been a somewhat doubtful mineral species. A tlapallite-like arsenate was also found from the Masonic district, California, USA, but it cannot be described at this time because the crystal blades are too small. This article focuses mainly on a cotype tlapallite specimen (180.92) and new material from the Wildcat prospect.

The specimen of tlapallite from which the single crystal was isolated for X-ray diffraction analysis was collected from the

Table 2. X-ray powder diffraction data for tlapallite to 60°2 θ (Wildcat) and 80°2 θ (cotype). Cutoff: averaged 10% intensities.

Cotype; CuK α		Wildcat, MoK α		Calculated		
I_{obs}	d_{obs}	I_{obs}	d_{obs}	d_{calc}	I_{calc}	$h\ k\ l$
7	11.905	39	12.014	11.932	60	0 0 1
13	5.955	31	5.981	5.966	37	0 0 2
14	4.750	25	4.778	4.761, 4.761	5, 23	1 0 2, 0 1 2
13	4.547	14	4.578	4.561	14	1 1 0
14	4.256	21	4.268	4.260	19	1 1 1
16	3.938	14	3.967	3.950	11	2 0 0
35	3.739	41	3.753	3.750, 3.750	20, 21	2 0 1, 0 2 1
17, 22	3.614, 3.545	42	3.575	3.623, 3.552, 3.552	15, 7, 34	1 1 2, 1 0 3, 0 1 3
26	3.285	30	3.301	3.293, 3.293	17, 15	2 0 2, 0 2 2
51	2.991	100	3.004	2.998	100	1 1 3
94	2.888	79	2.903	2.897, 2.897	7, 70	2 1 1, 1 2 1
17	2.796	20	2.804	2.803, 2.803, 2.791, 2.791	10, 2, 4, 11	2 0 3, 0 2 3, 1 0 4, 0 1 4
68	2.663	68	2.671	2.670, 2.670	40, 19	2 1 2, 1 2 2
100	2.626	54	2.636	2.633	59	3 0 0
10	2.382	15	2.393	2.386, 2.380, 2.380	6, 2, 5	0 0 5, 2 0 4, 0 2 4
10	2.190	11	2.196	2.196, 2.196, 2.191	6, 3, 2	3 0 3, 0 3 3, 3 1 0
42	2.106	40	2.115	2.110, 2.110	22, 12	2 1 4, 1 2 4
13	1.973	21	1.982	1.978	12	2 2 3
22	1.943	10	1.953	1.948, 1.948	3, 8	4 0 1, 0 4 1
14	1.870	19	1.872	1.875, 1.875	9, 1	4 0 2, 0 4 2
4, 16	1.820, 1.807	15	1.822	1.822, 1.812	11, 4	1 1 6, 3 2 0
52	1.787	23	1.795	1.792, 1.792	4, 14	3 2 1, 2 3 1
38	1.764	32	1.769	1.766, 1.766	13, 5	3 1 4, 1 3 4
43, 50	1.729, 1.719	41	1.731	1.734, 1.734, 1.724	12, 4, 16	3 2 2, 2 3 2, 4 1 0
42	1.645	38	1.653	1.649, 1.649, 1.647	8, 2, 12	2 3 3, 2 2 5, 0 4 4

Key: I_{obs} are observed intensities, d_{obs} are observed d -values, d_{calc} and I_{calc} are calculated d -values and intensities.

Wildcat prospect, in the Drum Mountains, Utah, USA, on 8 September 2018 by four of the authors (OPM, SJM, MFC and JM). The green plates were recognised in a vugh after a larger rock was cracked into two pieces (see Fig. 1). The piece of the specimen used for single-crystal X-ray diffraction is registered in the collections of Natural History Museum of Los Angeles County (catalogue number 67231), while the other half is registered in the collections of Museums Victoria (M54548). The crystals (if present) are often overgrown and intergrown, making single-crystal studies very challenging. The tlapallite crystals on these specimens are the best that have ever been reported for the species. Tlapallite occurs as several clusters of emerald green plates, nestled in cavities amongst quartz and carlfriesite. Other associated minerals include calcite, khinite, hedyphane and eckhardtite (previously only identified at Otto Mountain, California; Kampf *et al.*, 2013b). The plates of tlapallite reach 150 μm in diameter. A strong cleavage is observed parallel to the plates, indicative of the layered nature of the tlapallite crystal structure.

The carlfriesite crystal used in the new structure refinement was removed from an 8 cm \times 7 cm \times 3 cm fragment of dark grey jasperoid matrix. A radial spray of crystals on this carlfriesite specimen is shown in Fig. 2. The specimen was collected by one of the authors (MFC) at the Wildcat prospect in 2014 and it is now deposited in collections of the Natural History Museum of Los Angeles County (catalogue number 67227).

Chemistry

Quantitative chemical analyses of cotype tlapallite were performed on a Cameca SX100 Electron Microprobe (wavelength-dispersive mode, 12 kV, 10 nA, 5 μm beam diameter and PAP matrix correction) at the Imaging and Analysis Centre, Core Research Laboratories, Natural History Museum, London. Results are recorded to only one decimal place for Cu, Zn, Te and Pb as

the low values of voltage and current used to reduce dehydration during analysis input less energy into the sample and, consequently, give lower counting statistics (and errors slightly greater than ± 0.1 wt.%) for these elements. Analyses on Wildcat tlapallite (67231) were performed at Caltech using a JEOL 8200 microprobe operating at 15 kV, 25 nA and using a 5 μm spot size. There are 4 grains consisting largely of tlapallite exposed in the polished surface of the section and probe analyses were obtained from 2 of them. A back-scattered electron image of one of these grains along with EDS analysis spots is shown in Fig. 3. The EDS showed the tlapallite blades to be homogeneous in composition.

No beam damage was observed during the microprobe analyses. The standards used for cotype tlapallite were: synthetic fayalite (Si), baryte (S), wollastonite (Ca), Cu₂O (Cu), sphalerite (Zn), gallium arsenide (As), TeO₂ (Te) and vanadinite (Pb); while standards for specimen 67231 were: galena (Pb), anorthite (Ca), Cu metal (Cu), Te metal (Te), antimony metal (Sb), sodalite (Cl) and anhydrite (S). There was insufficient tlapallite for CHN analyses; therefore, H₂O was calculated based on 6 H atoms per 41 O atoms in the formula unit, as determined by the crystal structure analysis (see below), with the rest of the cation content renormalised to obtain electroneutrality. The total average weight percent of tlapallite after including H₂O remained slightly low, at 97.18 wt.% for the cotype and 93.77 wt.% for specimen 67231, most likely due to the thinness of the tlapallite plates. Analytical results are given in Table 1. These major-element analyses concur with the original data presented by Williams and Duggan (1978).

The analyses show that tlapallite contains essential Ca, Cu, S and Te (both Te⁴⁺ and Te⁶⁺, as determined by the crystal structure) and that the stoichiometric ratios of these major elements concur with the original data presented by Williams and Duggan (1978). Pb substitutes for Ca and Zn (only present in cotype tlapallite) substitutes for Cu. Substitutions of Si and As for S were also detected for cotype tlapallite. A substitution

Table 3. Summary of information relating to data collection and structure refinement of tlapallite.

Crystal data	
Ideal chemical formula	$(\text{Ca}_{0.87}\text{Pb}_{0.13})_3\text{CaCu}_6\text{Te}_8^{4+}(\text{Te}_{0.87}^{6+}\text{Sb}_{0.13}^{5+})_2\text{O}_{30}(\text{SO}_4)_2 \cdot 3\text{H}_2\text{O}$
Crystal system, space group	Trigonal, $P321$
Temperature (K)	293
a , c (Å)	$a = 9.1219(17)$, $c = 11.9320(9)$
V (Å ³)	859.8(3)
Z	2
Calculated density (g cm ⁻³)	5.035
Radiation type and wavelength (Å)	MoK α , 0.71075
μ (mm ⁻¹)	14.637
Crystal dimensions (mm)	0.040 × 0.040 × 0.004
Reflections for cell refinement	660; 4.28–22.46° θ
Data collection	
Crystal description	Green partial hexagonal plate
Diffractometer	Rigaku R-Axis Rapid II
θ range (°)	3.093 to 23.241
Indices range of h , k , l	$-10 \leq h \leq 10$, $-10 \leq k \leq 10$, $-12 \leq l \leq 13$
Absorption correction	Empirical multi-scan; <i>ABSCOR</i> (Higashi, 2001)
T_{\min} , T_{\max}	0.592, 0.944
No. of measured, independent and observed [$I > 2\sigma(I)$] reflections	4092, 832, 786
R_{int}	0.0812
Data completeness to $23.241^\circ\theta$ (%)	99.4
Refinement	
Number of reflections, parameters, restraints	832, 102, 1
$R_1[I > 2\sigma(I)]$, $R_2(\text{all})$	0.0296, 0.0329
$wR_2[I > 2\sigma(I)]$, $wR_2(\text{all})$	0.0608, 0.0625
GoF (F^2)	1.071
$\Delta\rho_{\min}$, $\Delta\rho_{\max}$ (e Å ⁻³)	-1.220, 0.848

of Sb, assumed to be Sb^{5+} substituting for Te^{6+} (as in joëlbruggerite, Mills *et al.*, 2009b), was detected for specimen 67231. The empirical formula for cotype tlapallite (180.92) is $\text{Ca}_{3.86}\text{Pb}_{0.53}\text{Cu}_{5.48}\text{Zn}_{0.53}\text{Te}_{8.19}\text{Te}_{2.05}^{4+}\text{S}_{1.56}\text{As}_{0.13}\text{Si}_{0.04}\text{H}_{6.00}\text{O}_{41.00}$, which can be expressed as $(\text{Ca}_{3.86}\text{Pb}_{0.53})_{\Sigma 4.39}(\text{Cu}_{5.48}\text{Zn}_{0.53})_{\Sigma 6.01}\text{Te}_{8.19}^{4+}\text{Te}_{2.05}^{6+}(\text{S}_{1.56}\text{As}_{0.13}\text{Si}_{0.04})_{\Sigma 1.73}\text{H}_{6.00}\text{O}_{41.00}$, while for specimen 67231, the empirical formula is $\text{Ca}_{3.82}\text{Pb}_{0.12}\text{Cu}_{6.56}\text{Te}_{7.97}\text{Te}_{1.59}\text{Sb}_{0.25}^{5+}\text{S}_{2.06}\text{H}_{6.00}\text{O}_{41.00}$, which can be expressed as $(\text{Ca}_{3.82}\text{Pb}_{0.12})_{\Sigma 3.94}\text{Cu}_{6.56}\text{Te}_{7.97}^{4+}(\text{Te}_{1.59}\text{Sb}_{0.25}^{5+})_{\Sigma 1.84}\text{S}_{2.06}\text{H}_{6.00}\text{O}_{41.00}$. The ideal end-member formula, based on the H_2O content inferred from crystal structure determination is $\text{Ca}_4\text{Cu}_6\text{Te}_8^{4+}\text{Te}_2^{6+}\text{O}_{30}(\text{SO}_4)_2 \cdot 3\text{H}_2\text{O}$. This requires CaO 8.82, CuO 18.76, TeO_2 50.19, TeO_3 13.81, SO_3 6.29 and H_2O 2.12, total 100 wt.%.

Raman spectroscopy

Raman spectra were recorded from a fine-grained crystalline aggregate of cotype tlapallite (180.92) using a Renishaw inVia spectrometer (Monash University) with an argon ion laser excitation operating at 514 nm. The spot was ~ 1 μm in diameter, with a 20 cm^{-1}/s scan rate and ~ 1 mW at the sample when using 10% laser power. This high-quality spectrum was used for comparison purposes.

At Caltech, a Renishaw M-1000 spectrometer with a 514 nm solid-state laser was used in most of the Te-oxysalt scanning. Most scanning was done at 10% power and 20 \times magnification resulting in a 5 μm spot size. A polarisation scrambler was used to minimise polarisation effects and the energy scale was

calibrated with silicon at 520.5 cm^{-1} . Spectra from the microprobe polished section of tlapallite were obtained on a Renishaw inVia spectrometer also using a 514 nm solid-state laser and a polarisation scrambler. This spectrometer was also calibrated with a silicon standard and was equipped with a low-wavenumber filter that allowed spectra to be recorded down to 10 cm^{-1} .

Spectra from the fine-grained Moctezuma cotype sample, the Otto Mountain fine-grained sample, and the North Star fine-grained sample are almost identical. We have recorded spectra from many different crystals in the Wildcat microprobe sample and, as might be expected when scanning different crystal orientations, they show variation in relative peak heights as well as lesser variations in the positions of some peaks; however, all are recognisable as tlapallite. The four spectra are shown between 100 and 1500 cm^{-1} in Fig. 4a. The lines at 710 and 798 cm^{-1} are in the ranges typically expected for tellurate and tellurite, while the lines at 975 cm^{-1} and 1106 cm^{-1} are in the range typically expected for sulfate. inVia data on the microprobe sample show that significant lines also occur at 58 and 91 cm^{-1} and that no other lines are present down to 10 cm^{-1} . The broad, fairly weak feature at ~ 1600 cm^{-1} is at twice the shift of the strongest Raman line, suggesting that it could be due to a second-order Raman process. It is also in the range commonly observed for water bending but appears to be stronger than expected for that.

There are also two features beyond 2800 cm^{-1} . The very broad water-stretching feature between 3220 and 3540 cm^{-1} has the same shape in the randomly oriented Moctezuma and Otto Mountain (Fig. 4b) samples. This feature can be reasonably interpreted as moderately strongly hydrogen-bonded water. The feature between 2860 and 2950 cm^{-1} can be reasonably described as a strongly hydrogen-bonded water molecule; the value of the $D\cdots A$ distance calculated using the equation of Libowitzky (1999) is 2.630 Å, within 2.5% of the $D\cdots A$ distance (2.689 Å) observed in the crystal structure (Table 5). This closeness also contributes to the overbonding of the OW site in the crystal structure (see below).

Crystallography

Powder diffraction

A powder aggregate of tlapallite, containing very minor quartz and calcite impurities, obtained from the cotype specimen (180.92) was mounted on a Rigaku R-Axis Rapid II curved imaging plate diffractometer (*Rigaku Oxford Diffraction) at the Natural History Museum, London and a dataset collected using CuK α radiation to 80°2 θ . A Gandolfi-type randomised crystal movement was achieved by rotations on the φ and ω axes. Observed d_{hkl} and reflection intensities of the cotype pattern were derived by profile-fitting using the Pawley method (Pawley, 1981) as implemented in the *HighScore Plus* software (Degen *et al.*, 2014). The PXRD for Wildcat tlapallite was recorded on a Rigaku R-Axis Rapid II diffractometer using MoK α radiation at the Natural History Museum of Los Angeles County, with conditions otherwise identical to the cotype data collection. Observed d -values and intensities were derived by profile fitting using *JADE 2010* software (Materials Data, Inc, 2010). The unit-cell parameters refined for cotype tlapallite from the powder data are $a = 9.0971(3)$ Å, $c = 11.9135(8)$ Å and $V = 853.83(7)$ Å³, and for Wildcat tlapallite the cell parameters are $a = 9.12(2)$ Å, $c = 11.960(1)$ Å and $V = 861(2)$ Å³. Both patterns are in good agreement with the one calculated using *PowderCell*

Table 4. Atom coordinates, site occupancies and atomic displacement parameters (\AA^2) for tlapallite. All full occupancies except for Te1 and Ca2.*

Atom	x/a	y/b	z/c	U_{eq}	U^{11}	U^{22}	U^{33}	U^{23}	U^{13}	U^{12}
Te1*	0	0	0.21466(15)	0.0113(5)	0.0090(7)	0.0090(7)	0.0158(10)	0	0	0.0045(3)
Te2	0.084912(15)	0.41220(15)	0.31180(9)	0.0127(3)	0.0106(7)	0.0121(6)	0.0167(6)	-0.0004(5)	-0.0003(5)	0.0067(6)
Te3	$\frac{2}{3}$	$\frac{1}{3}$	0.10707(17)	0.0186(5)	0.0154(7)	0.0154(7)	0.0249(12)	0	0	0.0077(3)
Cu	0.3694(3)	0.3849(3)	0.13972(19)	0.0170(6)	0.0121(12)	0.0120(12)	0.0220(13)	-0.0029(9)	0.0008(10)	0.0025(11)
Ca1	0	0	$\frac{1}{2}$	0.018(2)	0.014(3)	0.014(3)	0.025(5)	0	0	0.0071(15)
Ca2*	0	0.2507(4)	0	0.0192(13)	0.015(2)	0.0183(17)	0.023(2)	-0.0010(8)	-0.0021(16)	0.0075(11)
S1	$\frac{2}{3}$	$\frac{1}{3}$	0.3992(6)	0.0160(17)	0.015(3)	0.015(3)	0.018(4)	0	0	0.0075(13)
O1	0.5031(16)	0.3014(16)	0.3569(11)	0.030(4)	0.019(8)	0.041(9)	0.032(8)	-0.003(6)	-0.007(6)	0.017(7)
O2	$\frac{2}{3}$	$\frac{1}{3}$	0.5228(16)	0.035(6)	0.047(9)	0.047(9)	0.010(11)	0	0	0.023(5)
O3	0.1614(13)	0.1712(13)	0.1182(9)	0.009(3)	0.003(6)	0.007(6)	0.010(6)	-0.003(5)	0.000(5)	-0.003(5)
O4	0.4755(15)	0.3019(15)	0.0278(10)	0.016(3)	0.013(7)	0.017(7)	0.014(6)	-0.005(5)	0.004(5)	0.004(5)
O5	-0.0022(15)	0.4079(14)	0.1679(10)	0.012(3)	0.022(7)	0.013(7)	0.011(6)	-0.008(5)	-0.009(5)	0.015(6)
O6	0.3044(14)	0.4658(15)	0.2664(10)	0.018(3)	0.015(7)	0.015(7)	0.016(7)	-0.004(5)	0.003(6)	0.002(6)
O7	-0.0017(13)	0.1635(14)	0.3170(8)	0.012(3)	0.016(7)	0.014(7)	0.007(6)	-0.003(5)	0.001(4)	0.009(6)
OW	0.256(2)	0.256(2)	$\frac{1}{2}$	0.035(6)	0.032(9)	0.032(9)	0.019(12)	-0.007(5)	0.007(5)	0.001(10)
H	0.341(19)	0.26(3)	0.458(15)	0.042						

*Te1 is 0.8661 occupied by Te, 0.1339 occupied by Sb, fixed based on EPMA; **Ca2 is 0.871(5) occupied by Ca, 0.129(5) occupied by Pb.

Table 5. Metal–oxygen bond lengths (\AA) for tlapallite.

Te1–O3 \times 3	1.906(10)	Te3–O4 \times 3	1.875(12)	S1–O1 \times 3	1.460(12)
Te1–O7 \times 3	1.934(10)	Te3–O5 \times 3	2.839(12)	S1–O2	1.47(2)
<Te1–O>	1.920	Te3–O1 \times 3	3.280(13)	<S–O>	1.472
		<Te3–O> _{short}	1.875		
Te2–O5	1.884(11)	<Te3–O> _{long}	3.060	Ca1–OW \times 3	2.34(2)
Te2–O6	1.887(11)			Ca1–O7 \times 6	2.649(10)
Te2–O7	1.995(11)	Cu–O6	1.903(12)	<Ca1–O>	2.546
Te2–O6	2.379(11)	Cu–O3	1.941(11)		
Te2–O2	3.026(13)	Cu–O5	1.985(11)	Ca2–O3 \times 2	2.398(11)
Te2–O1	3.103(13)	Cu–O4	2.006(12)	Ca2–O5 \times 2	2.470(11)
Te2–O1	3.121(13)	Cu–O4	2.360(12)	Ca2–O4 \times 2	2.500(12)
Te2–OW	3.4252(13)	Cu–O1	3.116(13)	Ca2–O3 \times 2	2.522(10)
Te2–O3	3.492(10)	<Cu–O _{eq} >	1.959	<Ca2–O>	2.473
<Te2–O> _{short}	2.036	<Cu–O _{ap} >	2.738		
<Te2–O> _{long}	3.233				
Hydrogen bonding					
Donor O	$d(D-H)$ (\AA)	$d(H\cdots A)$ (\AA)	$d(D\cdots A)$ (\AA)	<DHA ($^\circ$)>	Acceptor O
OW	0.89(7)	1.81(8)	2.689(16)	170(20)	O1

(Kraus and Nolze, 1996) from the single-crystal structure (shown in Table 2). The powder data as indexed by Williams and Duggan (1978) was incorrectly indexed as monoclinic with $a = 11.97 \text{ \AA}$, $b = 9.11 \text{ \AA}$, $c = 15.66 \text{ \AA}$, $\beta = 90.60^\circ$ and $V = 1707 \text{ \AA}^3$. The unit-cell parameters of tlapallite indicate that Williams and Duggan (1978) were working on the same mineral, but indexed the powder lines in a lower symmetry setting: $a_{1978} \approx c_{2019}$, $b_{1978} \approx a_{2019}$, $c_{1978} \approx \sqrt{3}a_{2019}$, $\beta_{1978} \approx 90^\circ$ and $V_{1978} \approx 2V_{2019}$.

Single crystal X-ray diffraction

Single-crystal X-ray diffraction studies for both tlapallite and carlfriesite were carried out at the Natural History Museum of Los Angeles County using a Rigaku R-Axis Rapid II curved imaging plate microdiffractometer, with monochromatic MoK α radiation. The Rigaku CrystalClear software package was used for processing the structure data, including the application of empirical multi-scan absorption corrections using ABSCOR (Higashi, 2001). Initial structure models were obtained by the charge-flipping method using SHELXT (Sheldrick, 2015b). SHELXL-2016 (Sheldrick, 2015a) was used for the refinement of the structures.

The Pb content of the Ca2 site was refined to 13%. Similar attempts to refine the Sb content of the Te1 site were unsuccessful, so the Sb:Te ratio was fixed based on EPMA. A difference-Fourier map revealed the location of one H site in the structure of tlapallite. The hydrogen atom position was refined with a soft restraint of 0.90(5) \AA on the O–H distance with the U_{eq} of the H set to 1.2 times that of the donor OW atom. The carlfriesite structure contains no H atoms. For tlapallite, data collection and refinement details are given in Table 3, atom coordinates and displacement parameters in Table 4, selected bond distances in Table 5 and a bond valence analysis in Table 6. For carlfriesite, data collection and refinement details are given in Table 7, atom coordinates and displacement parameters in Table 8, selected bond distances in Table 9 and a bond valence analysis in Table 10.

Crystal structure description

Tlapallite

The crystal structure of tlapallite (Figs 5–8) has no known synthetic analogue, notably including the phyllotellurate anion $[\text{Te}_3\text{Te}^{6+}\text{O}_{12}]^{12-}$ for the first time. Tlapallite forms a layered

Table 6. Bond valence sums (in valence units) for tlappallite.

	Te1*	Te2	Te3	Cu	Ca1	Ca2**	S1	H	Σ
O1		0.06 × 2↓	0.04 × 3↓	0.02			1.58 × 3↓	0.25 (acceptor)	2.01
O2		0.07					1.54		1.62
O3	1.02 × 3↓	0.02		0.49		0.32 × 2↓, 0.23 × 2↓			2.09
O4			1.23 × 3↓	0.41, 0.15		0.25 × 2↓			2.04
O5		1.21	0.12 × 3↓	0.43		0.27 × 2↓			2.02
O6		1.19, 0.36		0.54					2.10
O7	0.97 × 3↓	0.92			0.16 × 6↓				2.05
OW		0.03			0.35 × 3↓			1.07 × 2→	2.51
Σ	5.98	3.93	4.17	2.04	2.02	2.13	6.29	1.07	

*87% Te, 13% Sb (fixed in the crystal structure based on EPMA); **87 % Ca, 13% Pb (calculated from the crystal structure).

Table 7. Summary of information relating to data collection and structure refinement of carlfriesite.

Crystal data	
Ideal chemical formula	CaTe ₂ ⁴⁺ Te ⁶⁺ O ₈
Crystal system, space group	Monoclinic, <i>I</i> 2/ <i>a</i>
Temperature (K)	293
<i>a</i> , <i>b</i> , <i>c</i> (Å)	9.9866(7), 5.67205(19), 12.2351(14)
β (°)	111.913(7)
<i>V</i> (Å ³)	642.98(9)
<i>Z</i>	4
Calculated density (g cm ⁻³)	5.691
Radiation type and wavelength (Å)	MoKα, 0.71075
μ (mm ⁻¹)	14.327
Crystal dimensions (mm)	0.14 × 0.07 × 0.01
Reflections for cell refinement	500; 4.52–30.07°θ
Data Collection	
Crystal description	Blade
Diffractometer	Rigaku R-Axis Rapid II
θ range (°)	3.590, 30.024
Indices range of <i>h</i> , <i>k</i> , <i>l</i>	–11 ≤ <i>h</i> ≤ 14, –7 ≤ <i>k</i> ≤ 7, –17 ≤ <i>l</i> ≤ 17
Absorption correction	Empirical multi-scan; <i>ABSCOR</i> (Higashi, 2001)
<i>T</i> _{min} , <i>T</i> _{max}	0.239, 0.870
No. of measured, independent and observed [<i>I</i> > 2σ(<i>I</i>)] reflections	4142, 928, 874
<i>R</i> _{int}	0.0384
Data completeness to 30.024°θ (%)	99.8
Refinement	
Number of reflections, parameters, restraints	928, 57, 0
<i>R</i> ₁ [<i>I</i> > 2σ(<i>I</i>)], <i>R</i> ₁ (all)	0.0230, 0.0247
<i>wR</i> ₂ [<i>I</i> > 2σ(<i>I</i>)], <i>wR</i> ₂ (all)	0.0528, 0.0538
GoF (<i>F</i> ²)	1.298
Δρ _{min} , Δρ _{max} (e ⁻ Å ⁻³)	–1.07, 2.50

structure parallel to {001}. Te⁶⁺O₆ octahedra share corners with three Te⁴⁺O₄ disphenoids. The Te⁴⁺O₄ disphenoid is a distorted trigonal bipyramid centred on Te⁴⁺, with one of the equatorial oxygen atoms replaced by the lone pair of Te⁴⁺. One primary Te⁴⁺–O bond in the disphenoid is considerably longer than the other three (2.379(11) compared to 1.884(11), 1.887(11) and 1.995(11) Å), a feature observed in some '[3 + 1]' asymmetrical disphenoids (e.g. the Te4 site in β-Na₂Te₄⁴⁺O₉; Lee and Ok, 2014). Each disphenoid is corner-linked to two others in a 'trimeric' arrangement, building two infinite sheets in the *ab* plane. Between these two sheets are distorted Cu²⁺O₆ octahedra and Te⁴⁺O₃ trigonal pyramids. The Cu²⁺O₆ square pyramids are connected to each other *via* edge-sharing to form Cu₂²⁺O₁₀ dimers. Each Cu²⁺O₆ octahedron connects to a Te⁶⁺O₆ octahedron by corner-sharing an O3 atom and connects to two

Te⁴⁺O₄ disphenoids via a corner-sharing O6 with one and an edge-sharing of O5 and O6 with another. The Te⁴⁺O₃ trigonal pyramids link three Cu₂²⁺O₁₀ dimers *via* corner-sharing with the bridging O4 atoms of the dimers. CaO₈ polyhedra (comprising three-quarters of the Ca atom sites) are also found within the layers, which they reinforce by sharing oxygen ligands with Cu and all three Te sites.

The Cu site in tlappallite displays a rather extreme example of Jahn-Teller type distortion, in a [4 + 1 + 1] arrangement. The four square-planar Cu–O bonds have an average length of 1.959 Å, in agreement with short Cu–O bonds having an average length ≈1.97 Å (Eby and Hawthorne, 1993). The Cu–O bond to the near apex (O4) of the Cu²⁺O₆ octahedron within the main layer is relatively short at 2.360(12) Å, and it is this edge along which the Cu²⁺O₆ octahedra share faces. Cu also displays an extremely weak Cu–O bond to the other octahedral apex at 3.116(13) Å, which extends into the interlayer, as this O1 site is one of the four oxygen atoms strongly bonded to S in the SO₄ group. In fact, this O1 site is further from Cu than the nearest Te atom, the Te3 site of the Te⁴⁺O₃ trigonal pyramids, at a distance of 3.000(3) Å. The average long Cu–O bond length is 2.738 Å, longer than the expected ~2.44 Å of Eby and Hawthorne (1993), but within the upper bounds of Jahn-Teller distortion, in which the longest apical bonds may reach ~3.15 Å (Eby and Hawthorne, 1993).

The coordination environments around Te⁴⁺ cations in tlappallite display two different one-sided geometries. The coordination of the Te3 site has typical one-sided trigonal pyramidal geometry, with three short, strong Te⁴⁺–O4 primary bonds at 1.876(12) Å, in good agreement with the 1.911 ± 0.077 Å expected for the three short Te⁴⁺–O trigonal pyramidal bonds (Mills and Christy, 2013). Te3 forms six longer secondary bonds to more distant oxygen atoms, on the same side of the cation as the lone pair – which for this Te site does not seem to be highly stereoactive. Three of these are 2.839(12) Å in length and connect with the O5 site, which is involved in the edge-linking of Cu²⁺O₆ octahedra and Te⁴⁺O₄ disphenoids, while the other three are longer at 3.280(13) Å, extending into the interlayer to the O1 sites of the SO₄ tetrahedra. The other half of the Te⁴⁺ cations (the Te2 site) are in disphenoidal fourfold coordination as described above. The Te2 site also possesses five longer secondary bonds, ranging in length from 3.027(13) to 3.492(10) Å, linking the O3 site (shared by the trigonal pyramidal Te3 site and octahedral Cu²⁺), the OW site and some of the SO₄ oxygen atoms. The lone pair of the Te2 site is more stereoactive than that of Te3 and is oriented into the interlayer channels. There is an average of 5.5 secondary bonds for the two Te⁴⁺ cations, in the expected range for Te⁴⁺ secondary bonds (Christy and Mills, 2013). The Te⁶⁺ site (Te1) displays typical octahedral coordination, with

Table 8. Atom coordinates, site occupancies and atomic displacement parameters (\AA^2) for carlfriesite. All sites fully occupied.

Atom	x/a	y/b	z/c	U_{eq}	U^{11}	U^{22}	U^{33}	U^{23}	U^{13}	U^{12}
Te1	$\frac{1}{2}$	$\frac{1}{2}$	$\frac{1}{2}$	0.00585(11)	0.00538(18)	0.0060(2)	0.00688(16)	−0.00051(12)	0.00316(13)	−0.00029(11)
Te2	0.85767(3)	0.58770(4)	0.71576(2)	0.00833(10)	0.00721(15)	0.00797(16)	0.00966(14)	−0.00033(9)	0.00298(10)	0.00069(8)
Ca	$\frac{1}{4}$	−0.4399(2)	0	0.0087(2)	0.0099(5)	0.0078(5)	0.0083(5)	0	0.0034(4)	0
O1	0.5188(3)	0.2584(5)	0.4019(2)	0.0100(5)	0.0100(14)	0.0100(13)	0.0101(12)	−0.0022(10)	0.0040(10)	0.0001(10)
O2	0.6967(3)	0.4085(5)	0.6041(2)	0.0092(5)	0.0069(13)	0.0100(13)	0.0092(13)	−0.0036(10)	0.0012(11)	0.0001(10)
O3	0.5807(3)	0.7181(5)	0.4195(2)	0.0098(5)	0.0117(14)	0.0085(13)	0.0120(12)	0.0007(10)	0.0079(11)	−0.0013(10)
O4	0.7741(3)	0.8965(5)	0.6850(2)	0.0093(5)	0.0122(14)	0.0070(13)	0.0112(12)	0.0018(10)	0.0074(11)	0.0039(10)

Table 9. Metal–oxygen bond lengths (\AA) for carlfriesite.

Te1–O1 $\times 2$	1.877(3)	Te2–O4	1.916(3)	Ca–O4 $\times 2$	2.374(3)
Te1–O1 $\times 2$	1.934(3)	Te2–O2	1.961(3)	Ca–O1 $\times 2$	2.443(3)
Te1–O3 $\times 2$	1.971(3)	Te2–O4	2.100(3)	Ca–O2 $\times 2$	2.513(3)
<Te1–O>	1.927	Te2–O3	2.104(3)	Ca–O3 $\times 2$	2.520(3)
		Te2–O1	2.445(3)	<Ca–O>	2.463
		Te2–O1	2.899(3)		
		Te2–O3	3.380(3)		
		<Te2–O> _{short}	2.105		
		<Te2–O> _{long}	3.140		

Table 10. Bond-valence sums (in valence units) for carlfriesite.

	Te1	Te2	Ca	Σ
O1	$1.08 \times 2\downarrow$	0.31, 0.10	$0.27 \times 2\downarrow$	1.76
O2	$0.91 \times 2\downarrow$	1.00	$0.23 \times 2\downarrow$	2.14
O3	$0.98 \times 2\downarrow$	0.70, 0.03	$0.22 \times 2\downarrow$	1.94
O4		1.11, 0.71	$0.32 \times 2\downarrow$	2.15
Σ	5.95	3.97	2.08	

three $\text{Te}^{6+}\text{--O}$ bonds at 1.906(10) \AA and another three at 1.934(10) \AA , with an average length of 1.920 \AA , in excellent agreement with the 1.923 ± 0.041 \AA expected for $\text{Te}^{6+}\text{--O}$ bonds (Mills and Christy, 2013).

$\text{Ca}(\text{H}_2\text{O})_3\text{O}_6$ polyhedra (comprising the remaining quarter of the Ca sites), SO_4 tetrahedra and H_2O groups are found between the layers, which also incorporate several long $\text{Te}^{4+}\text{--O}$ secondary bonds from both Te^{4+} sites. Oxygen atoms in SO_4 tetrahedra also form the long vertex of the Cu^{2+}O_6 octahedra and secondary bonds to both of the Te^{4+} centres within the main framework. Thus, the polytellurate sheets and other strongly-bound polyhedra CuO_6 , SO_4 and TeO_3 form a double-layered structural unit $\{\text{Cu}_6[\text{Te}_3^{4+}\text{Te}_6^{6+}\text{O}_{12}]_2(\text{Te}^{4+}\text{O}_3)_2(\text{SO}_4)_2\}^{8-}$. The long Ca1–O bonds, in particular, are involved in linking the layers together along [001], although this interlayer contains weaker connecting bonds than the rest of the tlappallite structure, resulting in a strong {001} cleavage. Only one of the two H atom positions of the inter-layer H_2O groups is involved in a hydrogen bond. This H-bond from the OW site *via* the H atom is accepted by one of the O1 sites of the SO_4 tetrahedra, providing further stability within the interlayer, in addition to the $\text{Te}^{4+}\text{--O}$ secondary bonds and linking Ca–O bonds.

The oxidation states assigned to the elements are confirmed by bond-valence analysis (Table 6), using the parameters of Gagné and Hawthorne (2015) for all elements except Te

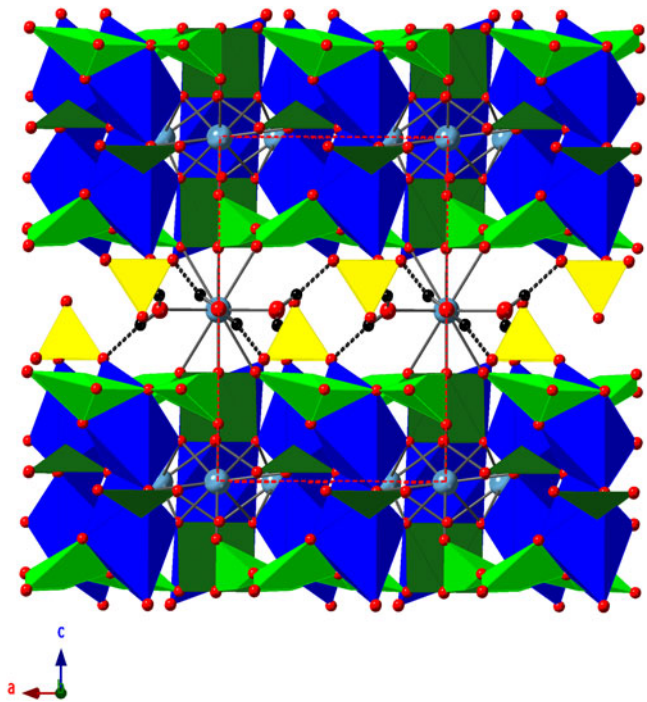


Fig. 5. The structure of tlappallite, showing stacking of two layers in the c direction. Cu^{2+}O_6 octahedra are in dark blue, Te^{4+} in dark green (surrounding oxygen atoms trigonal pyramidal) or in light green (surrounding oxygen atoms disphenoidal), SO_4 tetrahedra in yellow, Ca^{2+} cations in light blue, O atoms in red, and H atoms in black. H bonds are shown as dotted lines.

(Mills and Christy, 2013), Sb (Mills *et al.*, 2009a), Pb (Krivovichev and Brown, 2001) and H (Brown, 2002). The OW site is notably overbonded due in part to the short O–H distance (see above).

Carlfriesite

The nanoporous $[\text{Te}_2^{4+}\text{Te}^{6+}\text{O}_8]^{2-}$ framework structure of carlfriesite presented here (Figs 9–10) is identical in topology to that presented by Effenberger *et al.* (1978), in which a more detailed description of the structure and synthesis of carlfriesite are presented. Eight-coordinate Ca^{2+} cations are found within the channels. The stoichiometric Sr-analogue of carlfriesite, $\text{SrTe}_2^{4+}\text{Te}^{6+}\text{O}_8$, has since been synthesised (Weil and Stöger, 2007), although it contains a significantly different topology in its $[\text{Te}_2^{4+}\text{Te}^{6+}\text{O}_8]^{2-}$ framework, leading to narrower nanoporous channels than in carlfriesite, ~ 4 \AA in diameter compared to ~ 6 \AA (Christy *et al.*, 2016a).

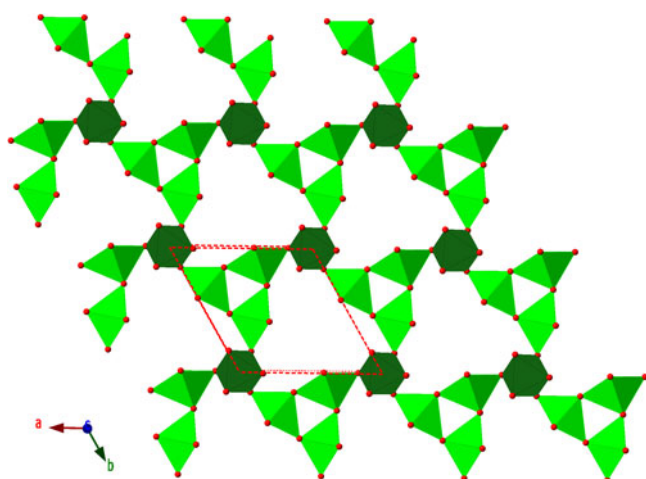


Fig. 6. The new sheet-forming phyllotellurate anion, $[\text{Te}_3^{4+}\text{Te}_6^{6+}\text{O}_{12}]^{12-}$. A portion of the infinite sheet formed by these anions is shown.

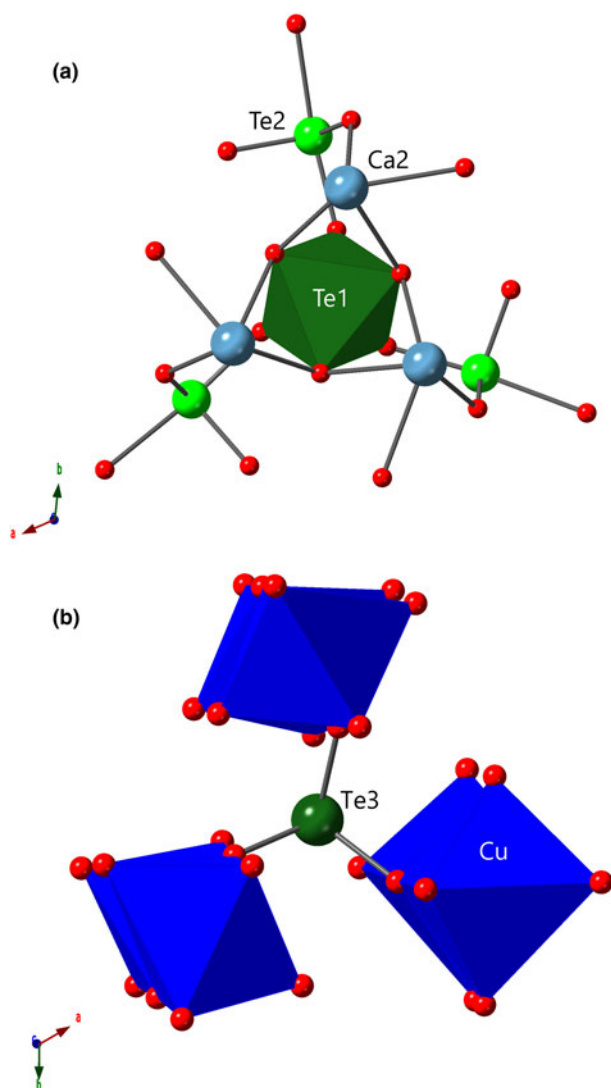


Fig. 7. Three-connecting sites in tlappallite. (a) Each $\text{Te}_6^{6+}\text{O}_{12}$ octahedron is linked to three $\text{Te}_4^{4+}\text{O}_4$ disphenoids and three Ca2 cations. (b) The trigonal pyramidal $\text{Te}_4^{4+}\text{O}_3$ bridges three $\text{Cu}_2^{2+}\text{O}_{10}$ dimers.

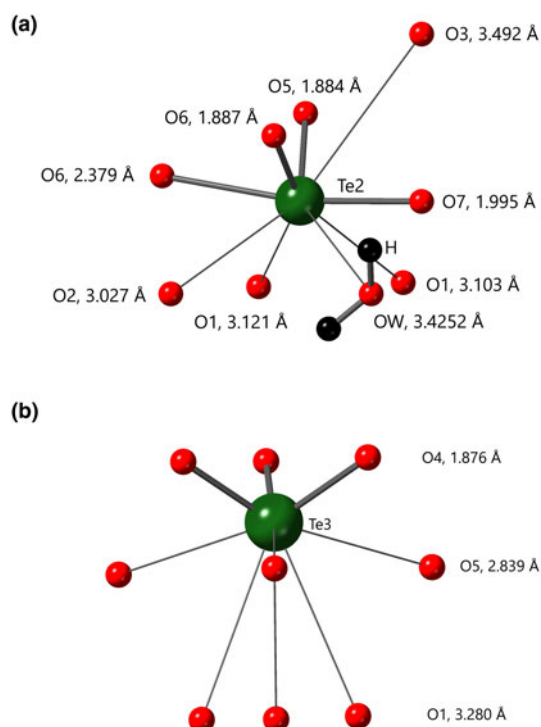


Fig. 8. Secondary bonding environments in tlappallite. (a) For $\text{Te}_4^{4+}\text{O}_4$ with four primary and five secondary bonds (noting that one secondary bond is on the same side as the primary), and (b) for $\text{Te}_4^{4+}\text{O}_3$ with three primary and six secondary bonds. Primary bonds are shown as thicker bonds with secondary as thin bonds.

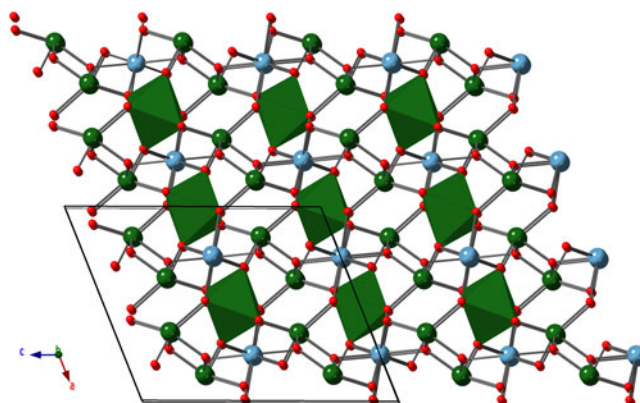


Fig. 9. The crystal structure of carlfriesite. $\text{Te}_6^{6+}\text{O}_{12}$ octahedra are shown in dark green, Te_4^{4+} cations in dark green, Ca^{2+} cations in light blue, and O atoms in red. Note that the Ca^{2+} cations fill pore space in the three-dimensional framework.

Both of these compounds are also enumerated and briefly (re-) described in the compendium of Te oxysalt structures compiled by Christy *et al.* (2016a).

Te_4^{4+} cations in carlfriesite form an unusual $\text{Te}_4^{4+}\text{O}_5$ network of primary bonds, with four bonds having lengths between 1.916(3) Å and 2.104(3) Å, and one longer primary bond to O1 at 2.445(3) Å. Te_4^{4+} in carlfriesite also possesses two secondary bonds at 2.899(3) and 3.380(3) Å, providing extra crosslinks within the nanoporous framework. The lone pairs of the Te_4^{4+} cations occupy the 5.091 Å space in the *a* direction between each $\text{Te}_4^{4+}\cdots\text{Te}_4^{4+}$ pair. Bond valence analysis (Table 10) for Ca (Gagné and Hawthorne, 2015)

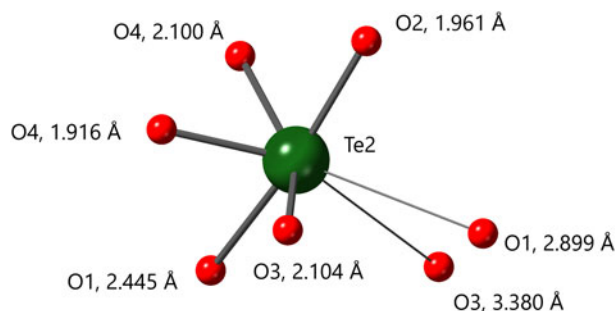


Fig. 10. Secondary bonding environments in carlfriesite. Primary bonds are shown as thicker bonds, secondary as thin bonds.

and Te^{4+} and Te^{6+} (Mills and Christy, 2013) concurs with the expected oxidation states for Ca, Te^{4+} and Te^{6+} in carlfriesite.

Relationships to other Te oxysalt structures

For either tlappallite or carlfriesite, there is no exact analogue in the catalogue of 703 Te oxycompounds with crystal structures compiled by Christy *et al.* (2016a), in which 26 mixed-valence Te oxysalts are reported. One of these 26 is the original carlfriesite refinement. No previously reported mixed-valence Te oxysalt contains Te^{4+} that is both trigonal prismatic and disphenoidal in its primary bonding. In addition, tlappallite also contains the first reported occurrence of the phyllotellurate anion, $[\text{Te}_3^{4+}\text{Te}^{6+}\text{O}_{12}]^{12-}$. As mentioned above, the Te environments in carlfriesite are different from those of tlappallite. Both carlfriesite and tlappallite display Te^{4+} dominance over Te^{6+} , with $\text{Te}^{4+}:\text{Te}^{6+}$ ratios of 2:1 and 4:1, respectively. Both minerals also contain calcium cations, although no synthetic mixed-valence Te oxysalt contains Ca. Tlappallite is the first mixed-valence Te oxysalt to also contain SO_4 (previous additional anions are limited to chloride and hydroxide in synthetic mixed-valence Te oxysalts). Tlappallite is similar to several other SO_4 -containing Te oxysalt minerals in that the SO_4 is found between layers composed of TeO_n polyhedra and MO_6 octahedra, where M is an octahedrally coordinated transition metal cation. A large-radius cation, such as Ca^{2+} or Pb^{2+} , also may be incorporated in the interlayer space with sulfate. Both tellurite- and tellurate-sulfate minerals are known with SO_4 in interlayer channels, including poughite (Gaines, 1968; Kampf and Mills, 2011) and bairdite (Kampf *et al.*, 2013a).

Supplementary material. To view supplementary material for this article, please visit <https://doi.org/10.1180/mgm.2019.9>

Acknowledgements. Equipment used in this study at Museums Victoria has been partly funded by The Ian Potter Foundation grant 'tracking tellurium' to SJM and a Museums Victoria 1854 Student Scholarship awarded to OPM, which we gratefully acknowledge. Equipment at the Natural History Museum of Los Angeles County was funded by the John Jago Trelawney Endowment. Support funding has also been provided to OPM by an Australian Government Research Training Program (RTP) Scholarship and a Monash Graduate Excellence Scholarship (MGES). Microprobe work on the cotype specimen was funded through Natural Environment Research Council grant NE/M010848/1 'Tellurium and Selenium Cycling and Supply' to Chris J. Stanley (Natural History Museum, London).

We thank Brendan Abrahams (University of Melbourne) and Joël Brugger (Monash University) for their insightful comments. We also thank Bill Birch (Museums Victoria) for his assistance in making the mount for EPMA analysis of the cotype, Finlay Shanks (Monash University) for his assistance in

acquiring the Raman data on cotype tlappallite and Jens Najorka (Natural History Museum, London) for help in acquiring the powder pattern on cotype tlappallite. The Raman spectroscopy at Caltech was done in the laboratory of George Rossman, and it and microprobe analyses at Caltech were supported by a grant from the Northern California Mineralogical Association. Three anonymous reviewers and Structures Editor Peter Leverett are thanked for their helpful comments, which improved the manuscript.

References

- Brown I.D. (2002) *The Chemical Bond in Inorganic Chemistry*. Oxford University Press, UK.
- Brugger J., Liu W., Etschmann B., Mei Y., Sherman D.M. and Testemale D. (2016). A review of the coordination chemistry of hydrothermal systems, or do coordination changes make ore deposits? *Chemical Geology*, **447**, 219–253.
- Christy A.G. and Mills S.J. (2013) Effect of lone-pair stereoactivity on polyhedral volume and structural flexibility: Application to $\text{Te}^{\text{IV}}\text{O}_6$ octahedra. *Acta Crystallographica*, **B69**, 446–456.
- Christy A.G., Mills S.J. and Kampf A.R. (2016a) A review of the structural architecture of tellurium oxycompounds. *Mineralogical Magazine*, **80**, 415–545.
- Christy A.G., Mills S.J., Kampf A.R., Housley R.M., Thorne B. and Marty J. (2016b) The relationship between mineral composition, crystal structure and paragenetic sequence: The case of secondary Te mineralization at the Bird Nest Drift, Otto Mountain, California, USA. *Mineralogical Magazine*, **80**, 291–310.
- Degen T., Sadki M., Bron E., König U. and Nénert G. (2014) The HighScore suite. *Powder Diffraction*, **29**, S13–S18.
- Eby R. and Hawthorne F. (1993) Structural relations in copper oxysalt minerals. I. Structural hierarchy. *Acta Crystallographica*, **B49**, 28–56.
- Effenberger H., Zemmann J. and Mayer H. (1978) Carlfriesite; crystal structure, revision of chemical formula, and synthesis. *American Mineralogist*, **63**, 847–852.
- Gagné O.C. and Hawthorne F.C. (2015) Comprehensive derivation of bond-valence parameters for ion pairs involving oxygen. *Acta Crystallographica*, **B71**, 562–578.
- Gaines R.V. (1968) Poughite, a new tellurite mineral from Mexico and Honduras. *American Mineralogist*, **53**, 1075–1080.
- Grundler P.V., Brugger J., Etschmann B.E., Helm L., Liu W., Spry P.G., Tian Y., Testemale D. and Pring A. (2013) Speciation of aqueous tellurium (IV) in hydrothermal solutions and vapors, and the role of oxidized tellurium species in Te transport and gold deposition. *Geochimica et Cosmochimica Acta*, **120**, 298–325.
- Higashi T. (2001) *ABSCOR*. Rigaku Corporation, Tokyo, Japan.
- Kampf A.R., Housley R.M., Rossman G.R., Marty J. and Chorazewicz M. (2018) Bodieite, $\text{Bi}_2^{3+}(\text{Te}^{4+}\text{O}_3)_2(\text{SO}_4)$, a new mineral from the Tintic district, Utah, and the Masonic district, California, USA. *The Canadian Mineralogist*, **56**, 1–10.
- Kampf A.R. and Mills S.J. (2011) The role of hydrogen in tellurites: Crystal structure refinements of juabite, poughite and rodalquilarite. *Journal of Geosciences*, **56**, 235–247.
- Kampf A.R., Mills S.J., Housley R.M., Rossman G.R., Marty J. and Thorne B. (2013a) Lead-tellurium oxysalts from Otto Mountain near Baker, California: X. Bairdite, $\text{Pb}_2\text{Cu}_4^{2+}\text{Te}_2^{6+}\text{O}_{10}(\text{OH})_2(\text{SO}_4)(\text{H}_2\text{O})$, a new mineral with thick HCP layers. *American Mineralogist*, **98**, 1315–1321.
- Kampf A.R., Mills S.J., Housley R.M., Rossman G.R., Marty J. and Thorne B. (2013b) Lead-tellurium oxysalts from Otto Mountain near Baker, California: XI. Eckhardtite, $(\text{Ca,Pb})\text{Cu}^{2+}\text{Te}^{6+}\text{O}_5(\text{H}_2\text{O})$, a new mineral with HCP stair-step layers. *American Mineralogist*, **98**, 1617–1623.
- Kampf A.R., Mills S.J. and Rumsey M.S. (2017) The discreditation of girdite. *Mineralogical Magazine*, **81**, 1125–1128.
- Kraus W. and Nolze G. (1996) POWDER CELL – a program for the representation and manipulation of crystal structures and calculation of the resulting X-ray powder patterns. *Journal of Applied Crystallography*, **29**, 301–303.

- Krivovichev S.V. and Brown I. (2001) Are the compressive effects of encapsulation an artifact of the bond valence parameters? *Zeitschrift für Kristallographie*, **216**, 245–247.
- Lee D.W. and Ok K.M. (2014) New polymorphs of ternary sodium tellurium oxides: hydrothermal synthesis, structure determination, and characterization of β - $\text{Na}_2\text{Te}_4\text{O}_9$ and $\text{Na}_2\text{Te}_2\text{O}_6 \cdot 1.5\text{H}_2\text{O}$. *Inorganic Chemistry*, **53**, 10642–10648.
- Libowitzky E. (1999). Correlation of O–H stretching frequencies and O–H...O hydrogen bond lengths in minerals. *Monatshefte für Chemie*, **130**, 1047–1059.
- Lindqvist O. and Moret J. (1973) The crystal structure of ditellurium pentoxide, Te_2O_5 . *Acta Crystallographica*, **B29**, 643–650.
- Marty J., Kampf A.R., Housley R.M., Mills S.J. and Weiß S. (2010) Seltene neue Tellurminerale aus Kalifornien, Utah, Arizona und New Mexico (USA). *Lapis*, **35**, 42–52.
- McPhail D. (1995) Thermodynamic properties of aqueous tellurium species between 25 and 350°C. *Geochimica et Cosmochimica Acta*, **59**, 851–866.
- Mills S.J. and Christy A.G. (2013) Revised values of the bond-valence parameters for $\text{Te}^{\text{IV}}\text{--O}$, $\text{Te}^{\text{VI}}\text{--O}$ and $\text{Te}^{\text{IV}}\text{--Cl}$. *Acta Crystallographica*, **B69**, 145–149.
- Mills S.J., Christy A.G., Chen E.C.-C. and Raudsepp M. (2009a) Revised values of the bond valence parameters for $^{[6]}\text{Sb(V)}\text{--O}$ and $^{[3-11]}\text{Sb(III)}\text{--O}$. *Zeitschrift für Kristallographie*, **224**, 423–431.
- Mills S.J., Kolitsch U., Miyawaki R., Groat L.A. and Poirier G. (2009b) Joëlbruggerite, $\text{Pb}_3\text{Zn}_3(\text{Sb}^{5+}, \text{Te}^{6+})\text{As}_2\text{O}_{13}(\text{OH}, \text{O})$, the Sb^{5+} analog of dugganite, from the Black Pine mine, Montana. *American Mineralogist*, **94**, 1012–1017.
- Mills S.J., Kampf A.R., Christy A.G., Housley R.M., Rossman G.R., Reynolds R.E. and Marty J. (2014) Bluebellite and mojaveite, two new minerals from the central Mojave Desert, California, USA. *Mineralogical Magazine*, **78**, 1325–1340.
- Materials Data, Inc. (2010) *JADE 2010 Complete XRD Analysis*. Livermore, CA, USA.
- Missen O.P., Mills S.J., Spratt J., Welch M.D., Birch W.D., Rumsey M.S. and Vylita J. (2018) The crystal structure determination and redefinition of eztlite, $\text{Pb}_2^{2+}\text{Fe}_3^{3+}(\text{Te}^{4+}\text{O}_3)_3(\text{SO}_4)\text{O}_2\text{Cl}$. *Mineralogical Magazine*, **82**, 1355–1367.
- Pasero M. (2018) The New IMA List of Minerals, <http://cnmnc.main.jp/>.
- Pawley G.S. (1981) Unit cell refinement from powder diffraction scans. *Journal of Applied Crystallography*, **14**, 357–361.
- Sheldrick G.M. (2015a) Crystal structure refinement with SHELXL. *Acta Crystallographica*, **C71**, 3–8.
- Sheldrick G.M. (2015b) SHELXT – integrated space-group and crystal-structure determination. *Acta Crystallographica*, **A71**, 3–8.
- Weil M. and Stöger B. (2007) Redetermination of SrTe_3O_8 from a hydrothermally grown single crystal. *Acta Crystallographica*, **E63**, i116–i118.
- Weil M., Shirkhanlou M. and Stürzer T. (2018) Phase formation studies of lead (II) copper (II) oxotellurates: The crystal structures of dimorphic PbCuTeO_5 , $\text{PbCuTe}_2\text{O}_6$, and $[\text{Pb}_2\text{Cu}_2(\text{Te}_4\text{O}_{11})](\text{NO}_3)_2$. *Zeitschrift für anorganische und allgemeine Chemie*, **645**, 347–353.
- Williams S.A. (1975) Xocomecatlite, $\text{Cu}_3\text{TeO}_4(\text{OH})_4$, and tlalocite, $\text{Cu}_{10}\text{Zn}_6(\text{TeO}_3)(\text{TeO}_4)_2\text{Cl}(\text{OH})_{25} \cdot 27\text{H}_2\text{O}$, two new minerals from Moctezuma, Sonora, Mexico. *Mineralogical Magazine*, **40**, 221–226.
- Williams S.A. (1979) Girdite, oboyerite, fairbankite, and winstanleyite, four new tellurium minerals from Tombstone, Arizona. *Mineralogical Magazine*, **43**, 453–457.
- Williams S.A. and Cesbron F.P. (1985) Yecoraite, $\text{Fe}_3\text{Bi}_5(\text{TeO}_3)(\text{TeO}_4)_2\text{O}_9 \cdot n\text{H}_2\text{O}$, a new mineral from Sonora, Mexico. *Boletín de Mineralogía*, **1**, 10–16.
- Williams S.A. and Duggan M. (1978) Tlapallite, a new mineral from Moctezuma, Sonora, Mexico. *Mineralogical Magazine*, **42**, 183–186.
- Williams S.A. and Gaines R.V. (1975) Carlfriesite, $\text{H}_4\text{Ca}(\text{TeO}_3)_3$, a new mineral from Moctezuma, Sonora, Mexico. *Mineralogical Magazine*, **40**, 127–130.